Thermal Spray

Meeting the challenges of the 21st Century

Proceedings of the
15th International Thermal Spray Conference
25-29 May 1998
Nice,France

Edited by
Christian Coddet

Organized by
Commissariat à l'Energie Atomique
Institut Polytechnique de Sevenans
Université de Limoges
Ecole Nationale Superieure des Mines de Paris
Ecole Centrale de Lyon
Institut de Soudure
on behalf of the
Select Committee
on Surfacing and Thermal Spraying
of the International Institute of Welding

Co-sponsored by
The ASM Thermal Spray Society
The German Welding Society
The High Temperature Society of Japan

Proceedings of the 15th International Thermal Spray Conference, 25-29 May 1998, Nice, France

SURFACE MORPHOLOGY OF PLASMA SPRAYED CERAMIC COATINGS

OKI S., GOHDA S., YAMAKAWA M.*
Kin-Ki University, OSAKA, JAPAN
*Kumano Technical College, MIE, JAPAN

Abstract

A novel method for characterization of microstructure of coatings is presented. Properties of plasma spray coatings are affected by their microstructure, which depends on the spraying conditions. Therefore, a detailed knowledge of microstructure is very important in order to know the coating formation mechanism and the properties of the coatings.

There are many studies to characterize the microstructure of coatings. In most of those studies, the microstructures are characterized from the polished cross-section of the coatings, and the results strongly depend on the preparation methods.

In this study, a new method for the characterization of coating microstructures by means of surface morphology is proposed. The distribution of shape and dimensions of splats were examined using quantitative analysis of scanning electron microscope images from the surface of the coatings.

The results indicate that the surface morphology strongly depends on the spraying conditions.

Keywords: characterization, coating property, splat morphology, equivalent diameter, shape factor

THERMAL SPRAY COATING is one of the engineering solution for wear and corrosion protection. Although, thermal spraying is widely used in many industrial applications, there are serious problems, such as low cohesive and adhesive strength and porosity. In order to improve the coating properties, it is important to know the influence of coating microstructure on mechanical properties and the relationships between spray parameters and microstructure of coating.

Properties of plasma spray coatings are affected by their microstructure, which depends on the spraying conditions. Therefore, a detailed knowledge of microstructure is very important in order to know the coating formation mechanism and the properties of the coatings.

There are many studies to characterize the microstructure of coatings[1, 2, 3]. However, in most of those studies, the microstructures are characterized from the polished cross-section of the coatings, and the results strongly depend on the preparation methods[1, 2].

This paper describes a new method for evaluating the coating microstructure by means of surface morphology. The distribution of shape and dimensions of splats were examined using quantitative analysis of scanning electron microscope images from the surface of the coatings.

Experimental Procedure

Material

The feedstock was a fused and crashed alumina powder (Al2O3, Japan Abrasive Co. Ltd., PC-WA-F) with the purity of 99.8 mass%. The particle size distribution, measured with a laser particle size analyzer, is shown in Table 1. The particle morphology, shown in Fig. 1, is angular, typical of a fused and crashed powder.

Processing Parameter

The powder was plasma sprayed in air using a Bay-

State P-120 gun (40kw type) onto plain carbon steel substrate (50 x 50 x 5 mm^3). The substrates were grit blasted with #24 alumina particles and alcohol rinsed. The spray parameters were listed in Table 2.

Table 1. Particle size distribution of feedstock.

10	15	20	30	40	50	60	μm
0.1	4.6	46.9	46.3	1.4	0.6	0.1	mass%

50 μm

Fig. 1. SEM image of feedstock alumina powder.

Table 2. Plasma spraying parameters.

Plasma Gas	Ar, 35 *l* / min
Arc Current	500, 600, 700 A
Arc Voltage	30, 31, 32 V
Spray Distance	70, 100, 130, 160 mm
Powder Gas	Ar, 3 *l* / min
Feeding Rate	25 g /min
Traverse Speed	90 mm / s, 5 mm / step

Characterization

Sprayed deposits were cross-sectioned, mounted in epoxy resin, ground and polished. Thickness of each specimen was measured from SEM images of these cross-sections. Porosity level was determined by image analysis. In addition, x-ray diffraction (XRD) patterns were taken from the surface of the coatings, to determine α / γ ratio of the coatings.

Surface Morphology

Surface morphologies were characterized by shape and dimension of each splat measured from SEM images of coating surface. The equivalent diameter, Deq, defined as the diameter of a circle with the same area as the selected feature, and the shape factor, Fs, defined as the ratio of periphery of the splat to the circumference of the circle with the same area. (Fig. 2) The equivalent diameter indicates the degree of flattening of splat, and the shape factor indicates the magnitude of peripheral material projections from the splats generated by impact. A series of 120 - 150 readings of each measurement was randomly located on the coating surface.

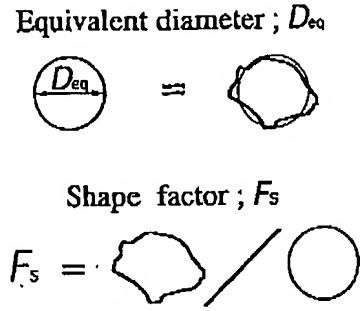

Fig. 2. Splat shape and size factors.

Results and Discussion

Properties of Coatings

Basic properties of the coatings, thickness, porosity and α / γ ratio of the coatings are shown in Fig. 3. Since the spraying distance affect those properties significantly, the properties were plotted against the spraying distance. The thickness of the coating was decreasing with the increasing of spraying distance. On the other hand, the porosity was increasing with the increasing of spraying distance. These results show that the deposition efficiency was decreasing with the increasing of spraying distance.

The α / γ ratio increased as the spray distance decreased. It is well known that alumina spray coating mainly consist of g-alumina because of rapid cooling of well melted particles. Cooling rate of the melted particles after impinging seems not to depend on the spraying distance markedly. Thus the increasing α / γ ratio caused by a decreasing spray distance may be due to particles that did not completely melt being incorporated in the coating/1/. The fact that the deposition efficiency was increasing with decreasing spraying distance is explained in terms of this mechanism.

Surface Morphology

Surface morphologies of each coating are shown in Fig. 4. It was found that splat morphologies varies with spraying distance. Figure 5 shows distribution of equivalent diameter of splats measured from the SEM image.

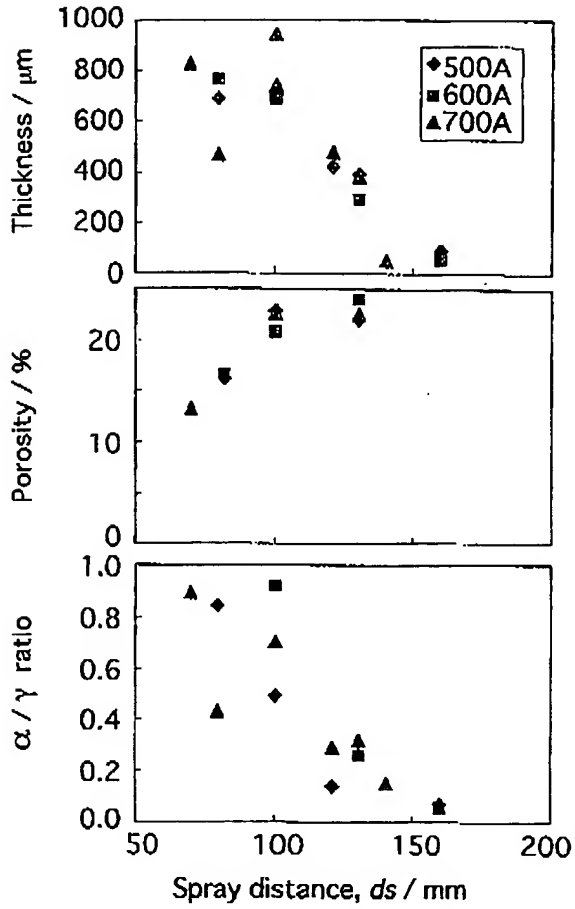

Fig. 3. Properties of coatings.

It seems to be no significant influence of spraying distance on the distribution of equivalent diameter. However, the range of distribution increased with decreasing spray distance, as shown in Fig. 6. The distribution profile of coating sprayed at 160mm was almost the same as that of the feedstock powder.

On the other hand, the distribution profiles of the shape factor, shown in Fig. 7, presented significant characteristics. That is, the shape factors moved to larger value as the spraying distance decreased. It means that the magnitude of peripheral material projects from the splats generated by impact increased with the decreasing of spraying distance, because of a low viscosity of melted particle just after impinging. If so, the degree of flattening of splat should be larger at the same time. However, as the spraying distance was decreased, the equivalent diameter spread not only to large diameter but also to small value. This may be due to a decrease of the mass of each splat caused by splashing, as well as secondary splat apart from primary splat.

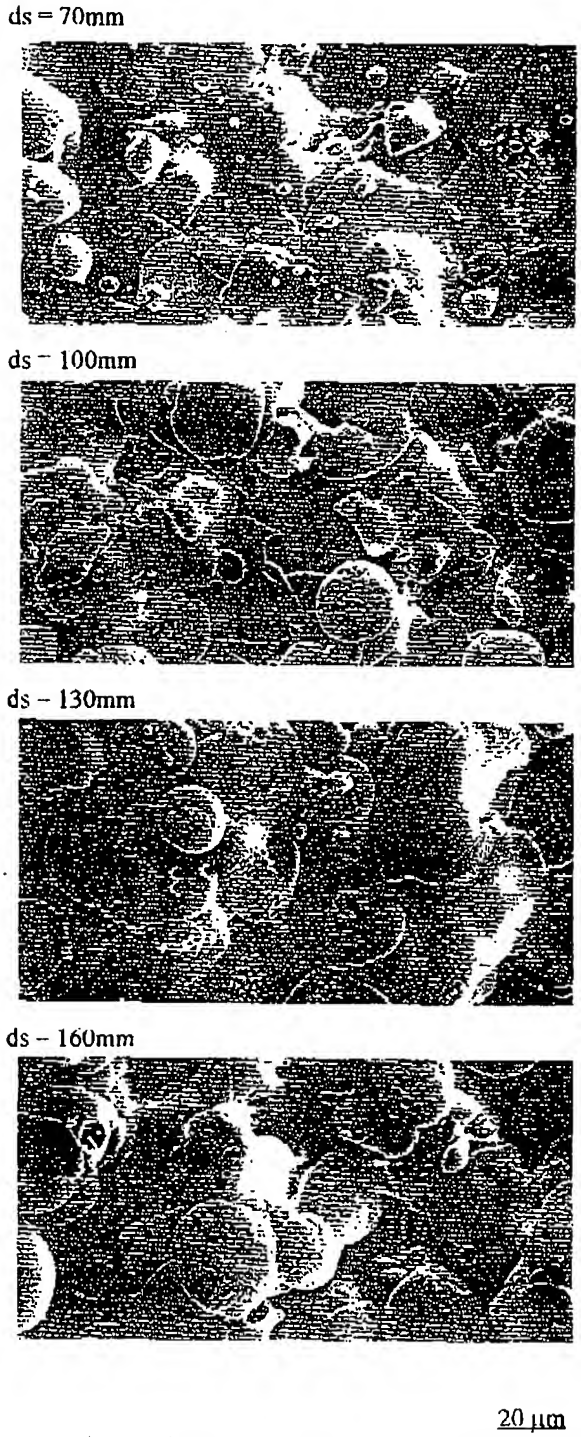

Fig. 4. Surface morphologies of coatings.

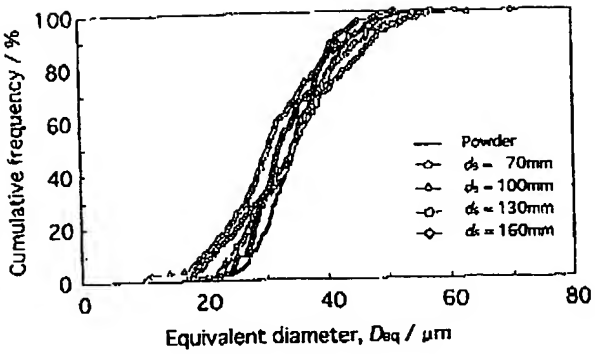

Fig. 5. Equivalent diameter, *D*eq, of coatings.

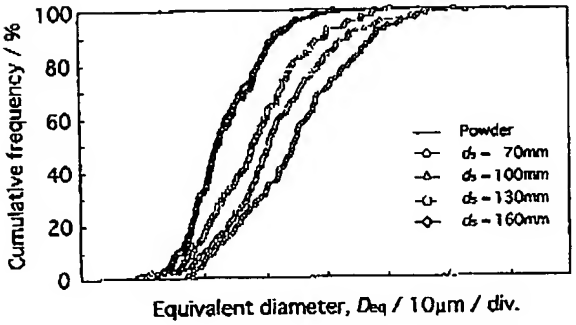

Fig. 6. Distribution of equivalent diameter, *D*eq.

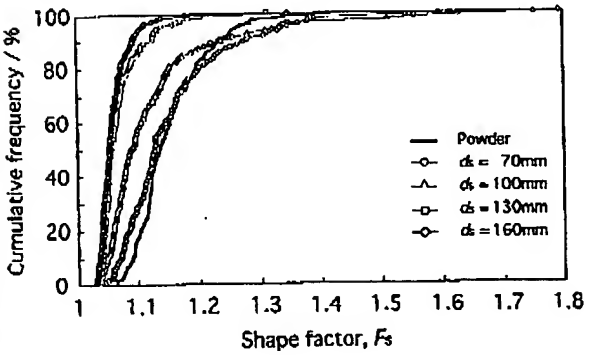

Fig. 7. Shape factor, *F*s, of coatings.

Figure 8 shows relationships between the shape factor and the equivalent diameter of each splat. This figure clearly suggests the mechanism of coating formation, as illustrated schematically in Fig. 9. Because of high viscosity of the particles sprayed at 160mm,

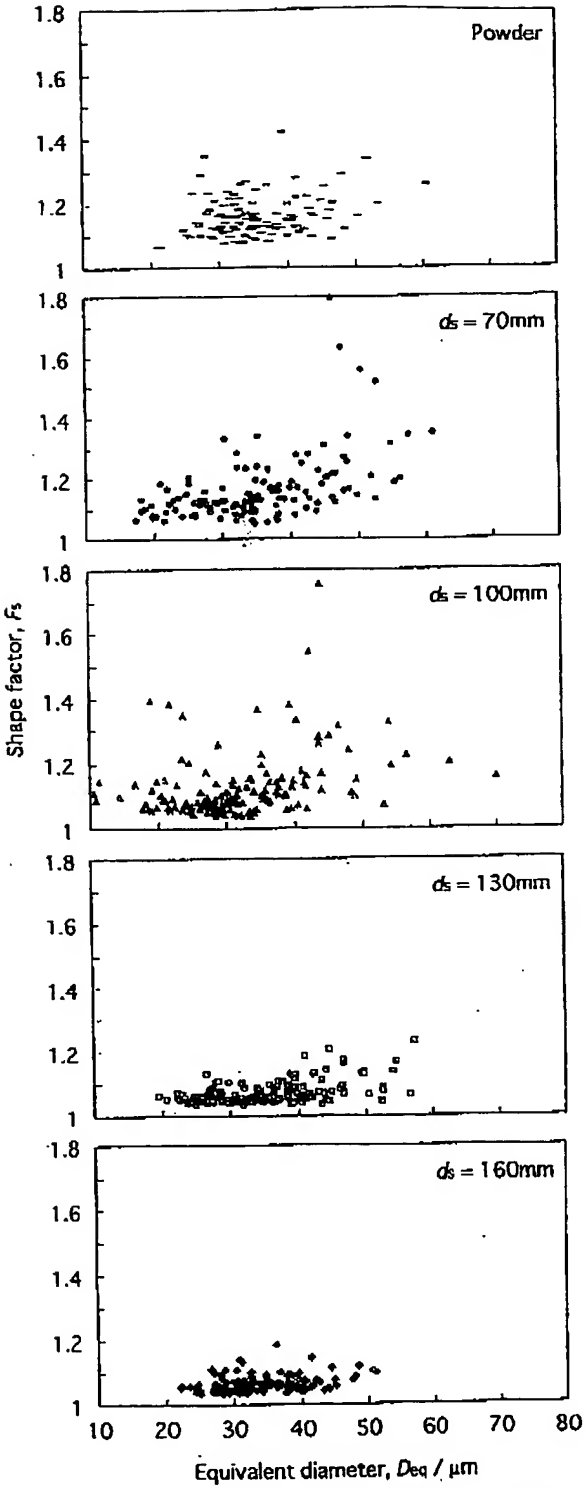

Fig. 8. Relationship between shape factor, *F*s, and equivalent diameter, *D*eq.

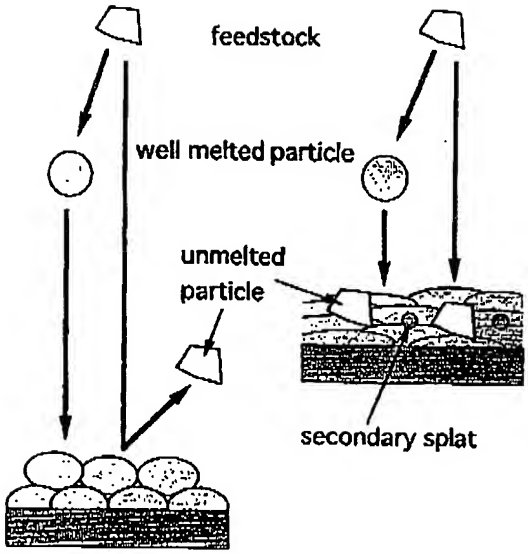

Fig 9. Schematic illustration of coating formation mechanism.

splats did not splash, did not flatten, and could not incorporate unmelted particles into the coating. This fact results the small value of shape factor with almost the same equivalent diameter as the feedstock material powder. On the other hand, as the small spray distance, splashing, flattening and incorporating of unmelted particles make wide variety of the equivalent diameter and the shape factor. This mechanism is consistent with high α / γ ratio of the coating sprayed at short spray distance.

Conclusion

A new method for the characterization of coating microstructures by means of surface morphology is proposed. The distribution of shape factor and equivalent diameter of splats were examined using quantitative analysis of scanning electron microscope images from the surface of the coatings. The results indicate that the surface morphology strongly depends on the spraying conditions, and the mechanism of coating formation can be suggested by the surface morphology.

References

1. C. Takahashi and T. Senda, Proc. ITSC95, (1995), pp. 921 - 926.
2. A. Ohmori and C.J. Li, Thin Solid Films, 201(1991), pp. 241 - 252.
3. G. Montavon, C. C. Berndt, C. Coddet, S. Sampath and H. Herman, JTST, 6(1997), pp. 153 - 166.

Thermal Spray

Surface Engineering via Applied Research

Proceedings of the
1st International Thermal Spray Conference

8–11 May 2000
Montréal, Québec, Canada

Edited by
Christopher C. Berndt

Sponsored by
ASM Thermal Spray Society
Deutscher Verband für Schweisstechnik
International Institute of Welding

ASM International®
Materials Park, OH 44073-0002

http://www.asm-intl.org

TSS
ASM Thermal Spray Society

DVS
German Welding Society
(Deutscher Verband für
Schweisstechnik - DVS)

iiw
iis
International
Institute of Welding

Splat Formation in Off-Normal Angle Spray

H. Fukanuma, Y. Huang
Plasma Giken Co., Ltd., Toda City, Saitam, Japan

Introduction

The thermal spray process in an off-normal angle spray has been little studied. Several studies on microstructure and mechanical properties of off-normal angle spray deposits have been reported [1-3]. Montavon et al studied the splat morphology of off-normal angle spraying and showed that the elongation ratio increases from approximately 1 to 2 when the spray angle changes from 90° to 30°, and that the average splat area is little influenced by the spray angle [4, 5]. The elongation ratio is defined as the ratio of the longest distance "*a*" to the shortest distance "*b*". The length "*a*" and "*b*" are shown in Fig.1. Montavon and Coddet investigated the 3D profile of the splat sprayed at off-normal angles. They reported that the splat thickness profile is inclined and that a lower spray angle induces a higher slope in the splat thickness [6].

A few numerical studies have been reported very recently. Sobolev et al reported the relationship between the flattening characteristic and the Reynolds number at off-normal spray angles [7]. They calculated the splat radius under a certain velocity field in the splat and the assumption of splat circularity at spray angles between 90° to 45°. They showed that, as the spray angle decreases, the splat radius increases and the particle pressure on the substrate surface during flattening decreases. Our previous study proposed a mathematical model that predicted the elongation ratio as a function of the spray angle by introducing a parameter "*n*" that influences the ratio of the parallel velocity to the perpendicular velocity of the particle to the substrate. The model agreed with the experimental results at spray angles of 90° to 30° [8]. Bussmann et al reported the simulation results of off-angle impact by employing the RIPPLE method [9]. Nickel particle impact in plasma and HVOF sprays were simulated in the study.

The aim of the present study is to examine the splat shape at off-normal angles in plasma spray and to investigate the relationship between the splat elongation ratio and the spray angle on various spray materials and particle sizes. The applicability of the model to the experimental results is investigated.

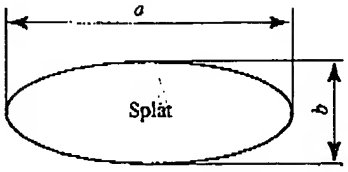

Fig. 1. The definition of the longest distance and shortest distance of a splat.

Experimental Procedure

In this study, six powders of aluminum, copper and nickel as metal spray materials, and alumina, titania and zirconia as oxide materials were sprayed, Table 1.

The substrate specimens were made of stainless steel. The dimensions of the specimen are shown in Fig. 2-a. The spray angle "φ" illustrated in Fig. 2-a was 90°, 75°, 60°, 45°, 30° and 15°. This is defined as the angle between the central axis of the torch and the surface plane of the specimen. Those six types of the specimen were arranged as shown in Fig. 2-b for plasma spraying.

In the study, the plasma spray torch was a SG-100 from Miller Thermal Company. The one-pass spray was made in the direction shown in Fig. 2-b. The spray parameters are listed in Table 2.

Table 1. Chemical composition and particle size range of the spray powder.

Material	Chemical Composition	Particle Distribution
Al	99% Al	< 106 μm
Cu	99.3% Cu	< 106 μm
Ni	99.8% Ni	45-105 μm
Al_2O_3	99% Al_2O_3	10~32 μm
TiO_2	99% TiO_2	10~45 μm
ZrO_2	93% ZrO_2, 4% CaO	5~45 μm

Table 2. Spray conditions for metals and oxides.

Parameter	Metal Material	Oxide Material
Arc Current	800 A	800 A
Arc Voltage	40 V	40 V
Arc Gas Flow Ar	40 l/min.	40 l/min.
He	20 l/min.	42.5 l/min.
Spray Distance	100 mm	100 mm
Torch Traverse Speed	800 mm/sec.	800 mm/sec.
Substrate Temperature	400 °C - 450 °C	

Results and Discussions

The shape of splats. Aluminum and alumina splats sprayed at angles of 90° to 15° are shown in Fig. 3 and 4, respectively, as typical examples. Figure. 3 shows that all aluminum splats have projections around peripheral regions at every spray angle. On the contrary, alumina splats have distinctive outlines, Fig. 4. Figures 3 and 4 show that splats of aluminum and alumina elongate as the spray angle decreases.

The profile of splats at an off-normal angle spray was found to be elliptic. Twenty splats of different materials that were sprayed at 75° to 15° were photographed and the lengths "a" and "b" of the splats shown Fig. 1 were measured from randomly selected photographs. The ellipse with the diameters that equate "a" and "b" of the splat was drawn on transparent paper and superimposed on the splat's photograph. Every splat was compared with the corresponding drawn ellipse. The results of nickel and zirconia splats are shown in Fig. 5. The elliptic contours are drawn with a dashed line in the figure. The figure shows that the splat profile fits its corresponding ellipse except for the peripheral projections around the splat. In particular, the contour lines of zirconia splats are clear. On the contrary the outlines of nickel splats are less distinct due to splashing in the downstream direction.

The relationship between "a" and "b". The long length and short length of splat "a" and "b" are defined as the major diameter and minor diameter of the ellipse, respectively, because splats can be characterized as an ellipse. Major diameter "a" and minor diameter "b" were measured on the splats of the six different materials at spray angles of 90° to 15°. Figures 6 shows that the relationship between the major diameter "a" and the minor diameter "b" of nickel splats is linear at every angle, 90° to 15°, and that the linear slope increases as spray angle decreases. Figure 7 and 8 show that aluminum and alumina have the same relationship as nickel.

The relationships between "a" and "b" of alumina, titania, zirconia and aluminum are illustrated in Fig. 9. The graph shows that these four different materials are nearly on the same line at each spray angle. Thus, the ratio "a/b" is not influenced by the chemistry of the materials. Figure 9 shows that "a" changes from around 50 μm to more than 1000 μm and "b" from less than 50 μm to around 400 μm. The linearity of the relationship between "a" and "b" holds over the wide range of splat sizes, that is, the ratio "a/b" does not depend on the splat size.

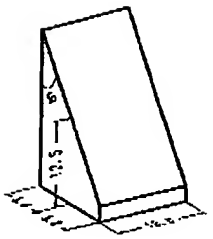

a. Specimen demensions

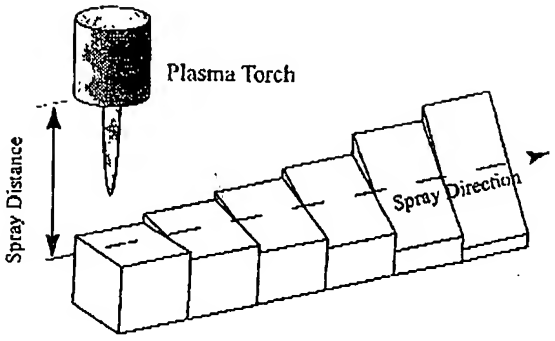

b. The specimem arramgement

Fig. 2. Specimen dimensions and arrangement for plasma spray.

The flattening process generally depends on the Reynolds number [10,11]. The Reynolds number is defined as:

$$\mathrm{Re} = \frac{\rho v_0 d_0}{\mu} \qquad (1)$$

Where ρ, v_0, d_0 and μ are the particle density, the velocity at impact, the diameter and viscosity, respectively. The flattened splat size is described as a function of the Reynolds number. The ratio "a/b" is independent on the splat size and implies it does not depend on the particle size, initial velocity and viscosity; that is, the ratio only depends on the spray angle.

The elongation ratio and the model. Montavon et al defined the ratio of "a" to "b" as the elongation ratio [4]. This term is also used to express "a/b" in this paper. Table 3 shows the experimental results as the average and standard deviation of the elongation ratio. The average elongation ratio increases as the spray angle decreases in all the materials. The standard deviation also rises as the spray angle is lowered. Each elongation ratio at 90° to 30° is very similar to the others; except at 15° as shown in Fig. 10.

The elongation ratio of copper is shown in Fig. 11 and that of titinia in Fig.12. The curves that were predicted by the

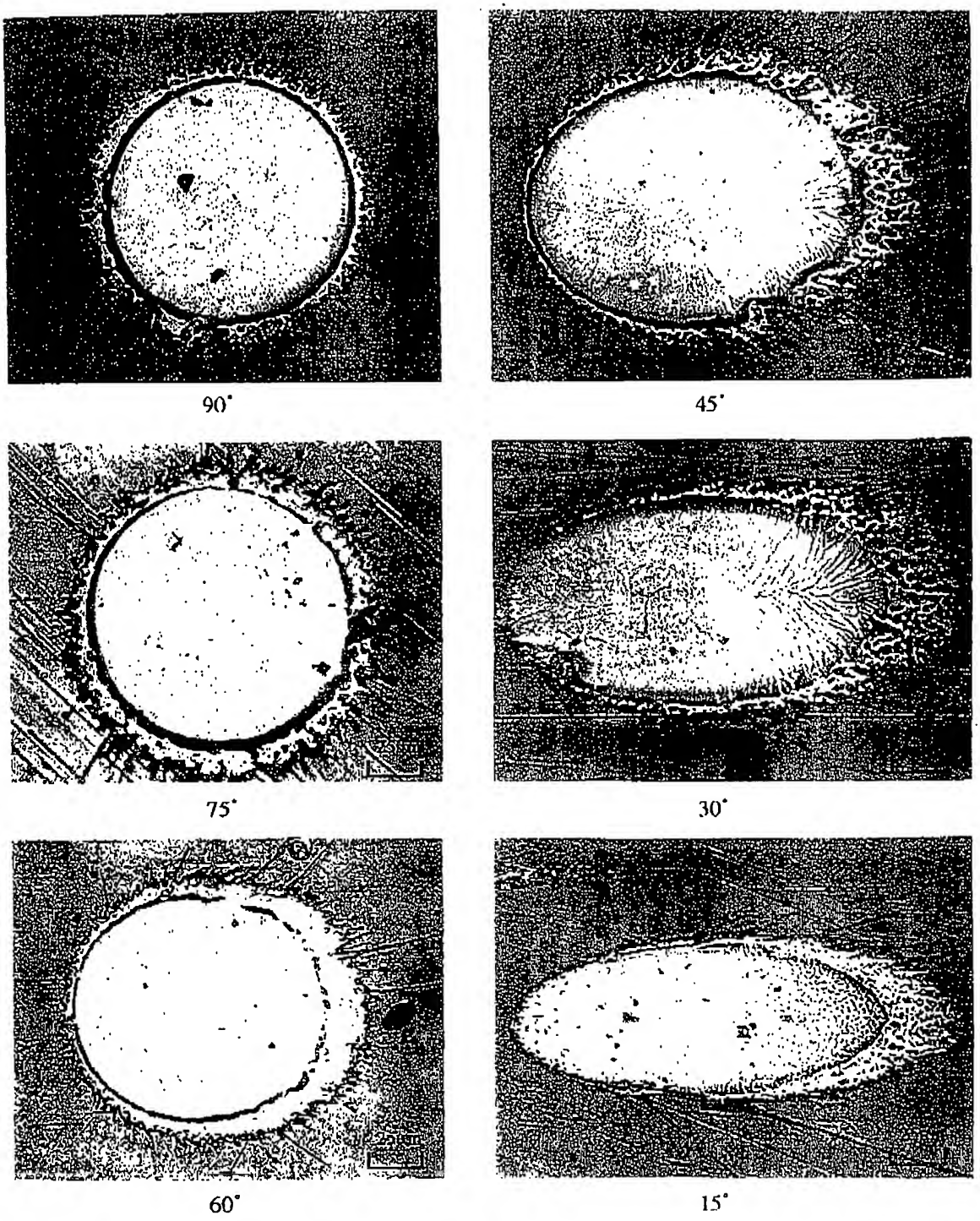

Fig. 3. Aluminum splats sprayed at angles 90° to 15°.

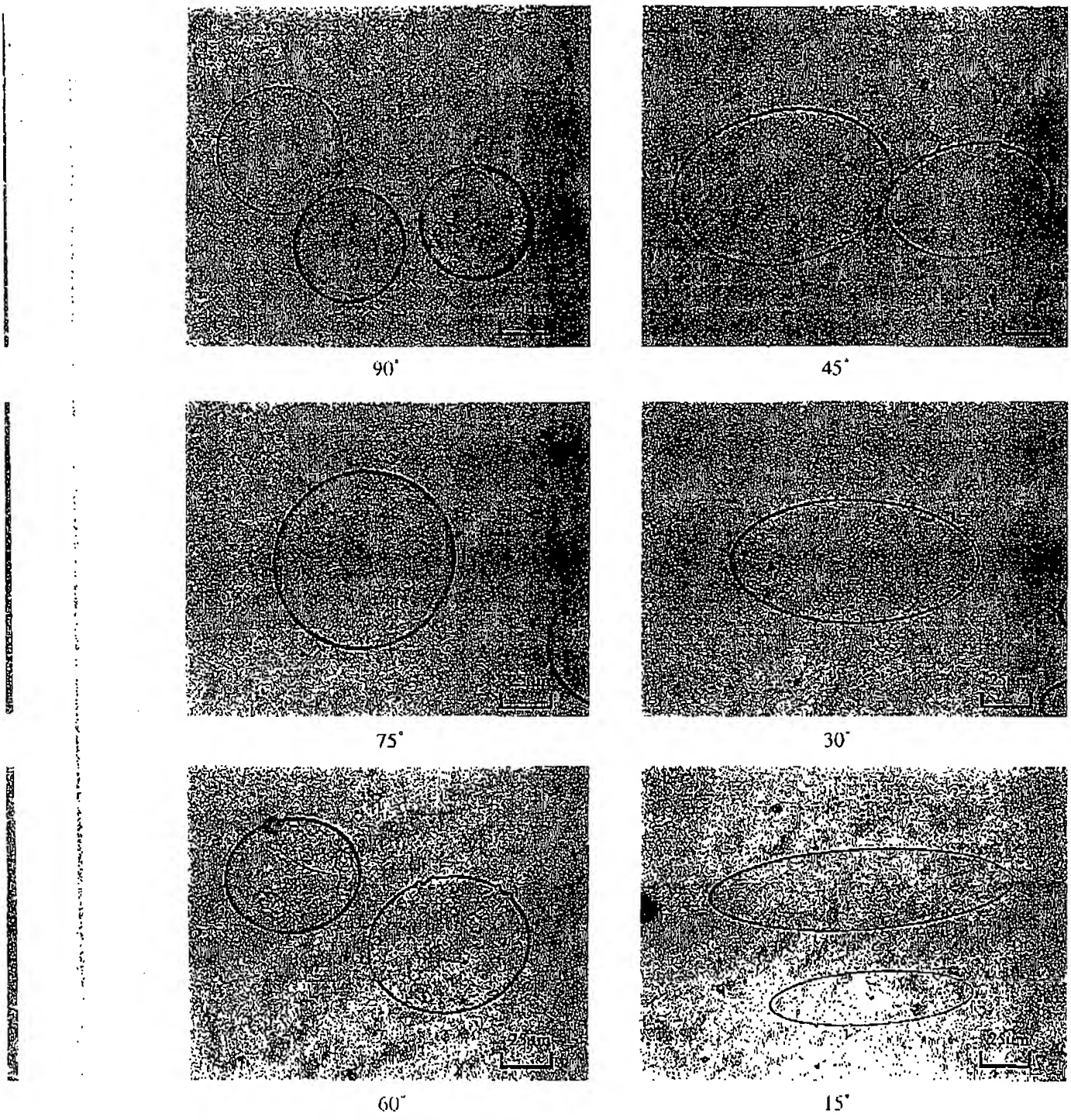

Fig. 4. Alumina splats sprayed at angles 90° to 15°.

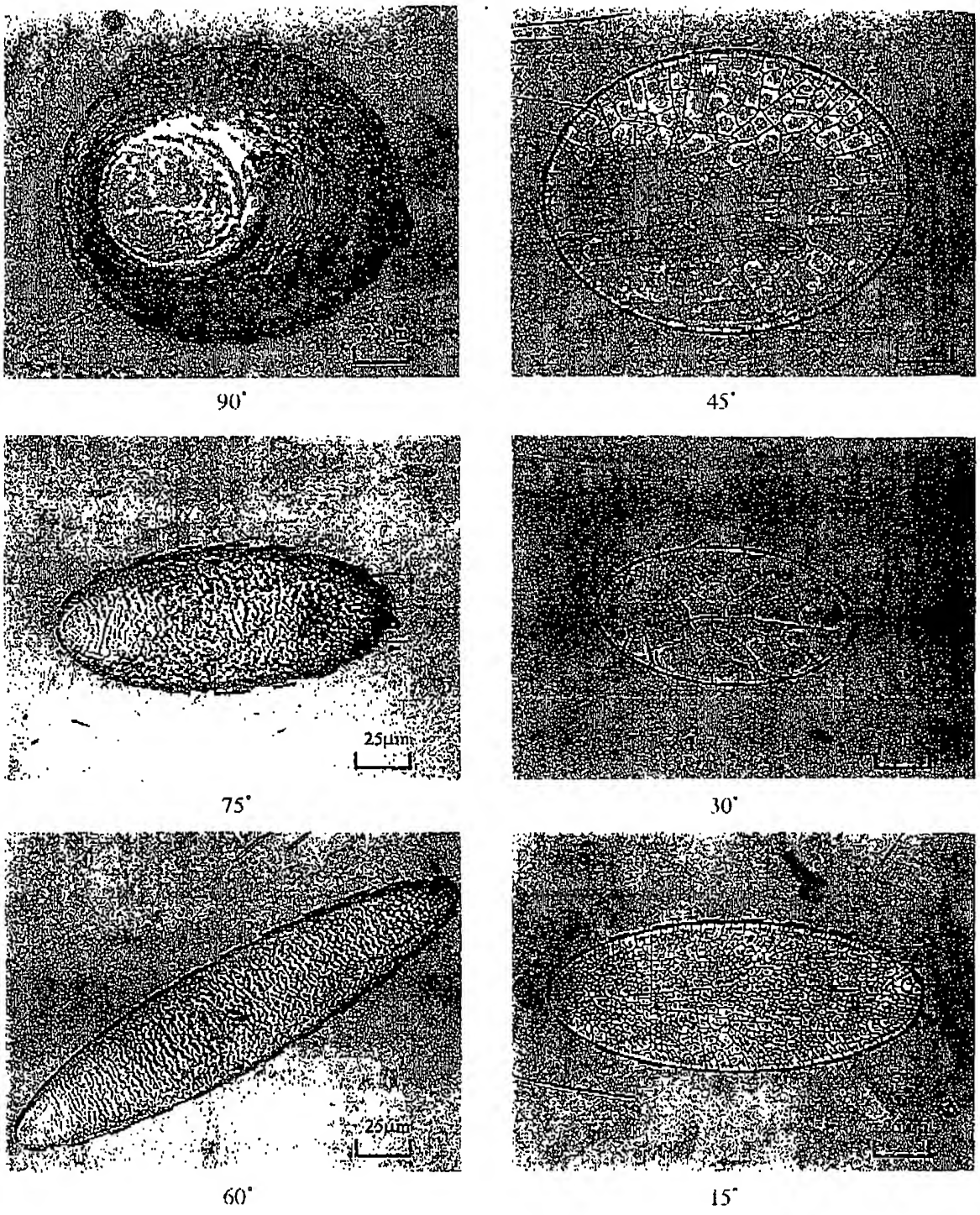

Fig. 5. The comparison of nickel and zirconia splat shapes with elliptic contour..

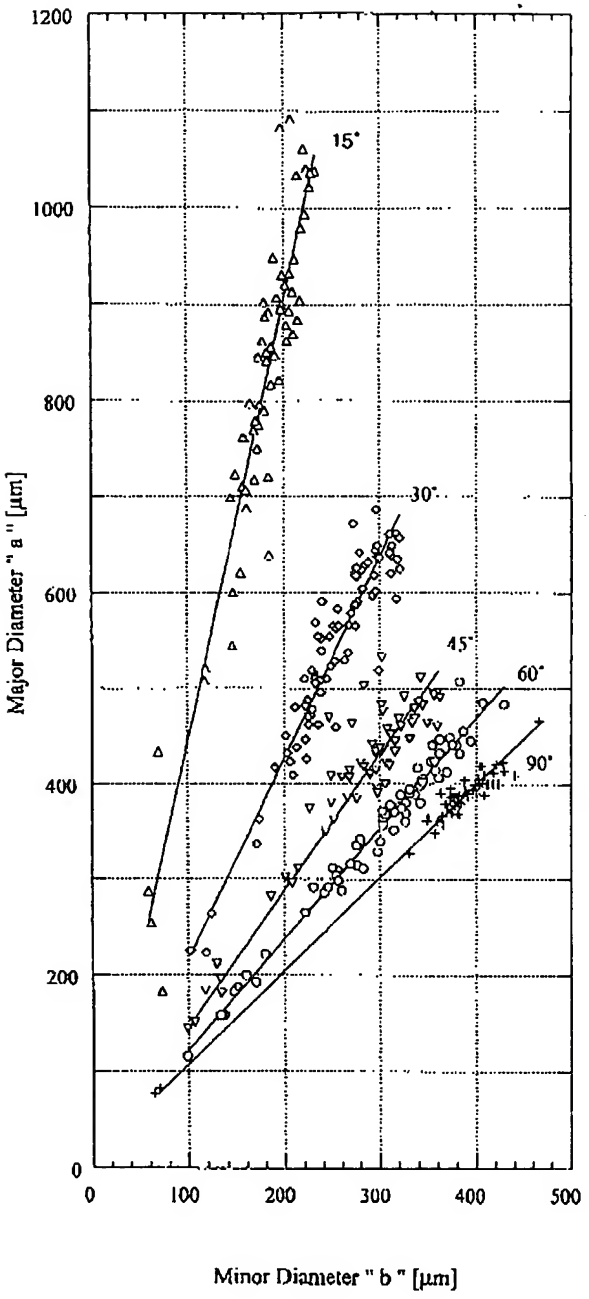

Fig. 6. The relationship of Nickel splat between the major diameter and the minor diameter at spray angles 90° to 15°.

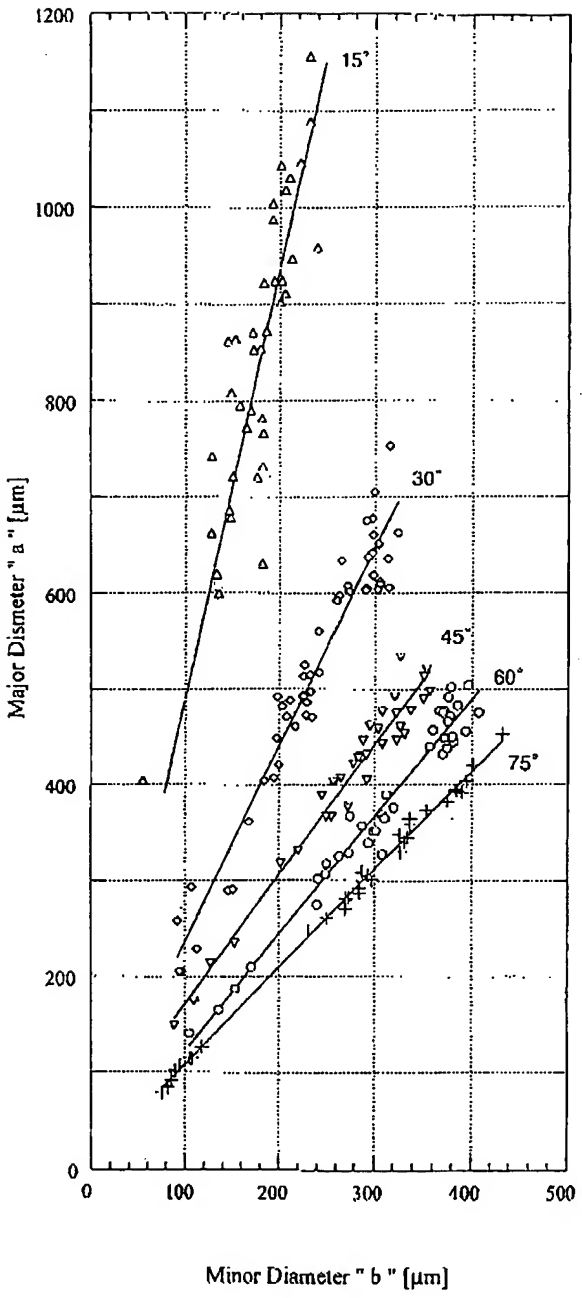

Fig. 7. The relationship of Aluminum splat between the major diameter and the minor diameter at spray angles 75° to 15°.

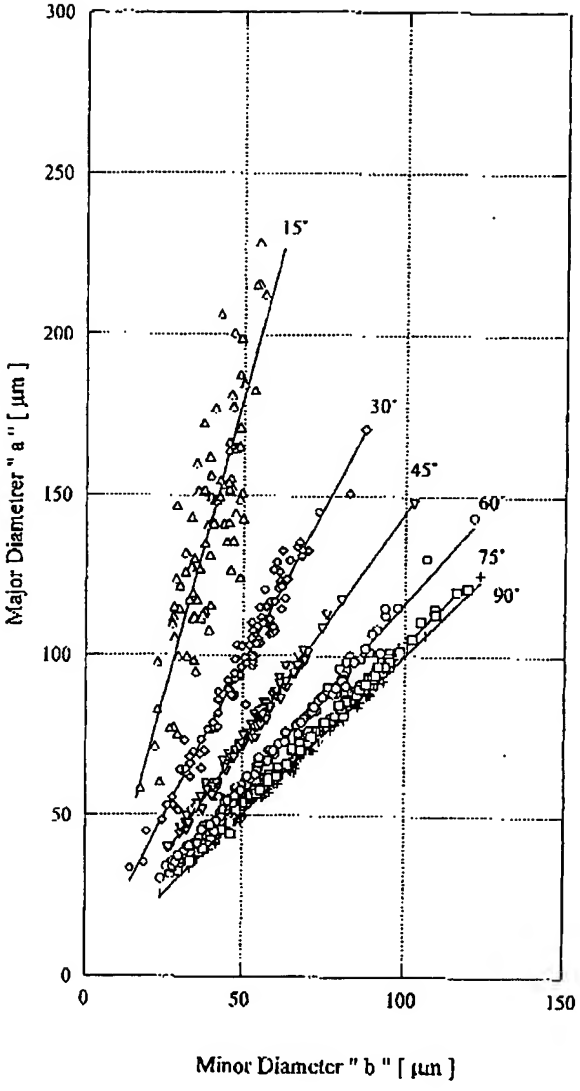

Fig. 8. The relationship of Alumina splat between the long diameter and the short diameter at spray angles 75° to 15°.

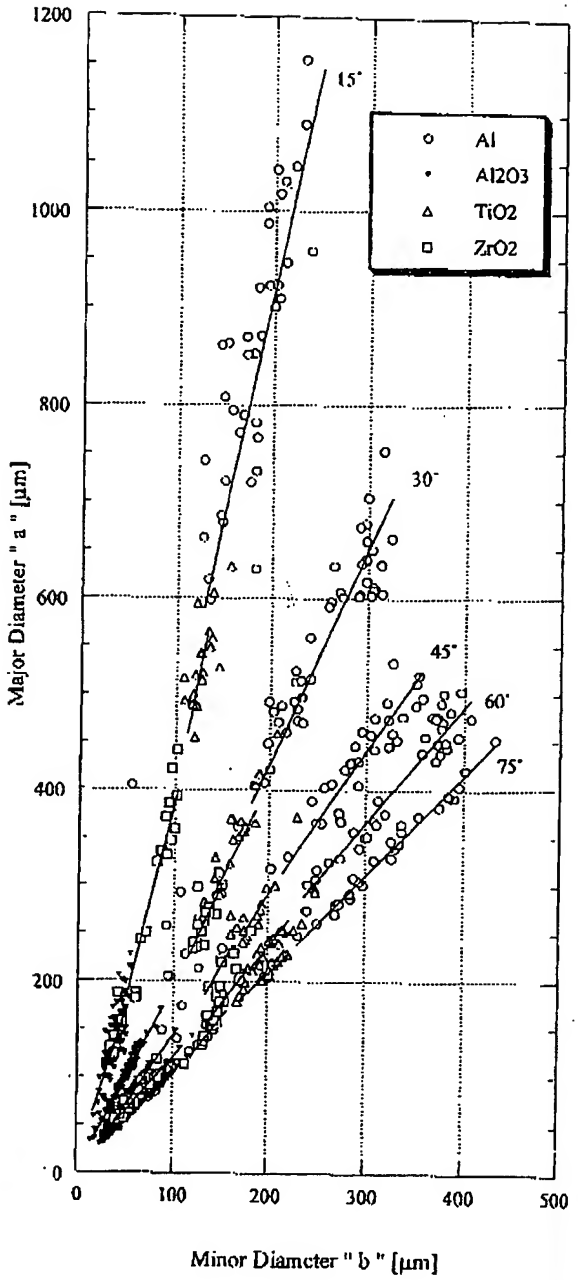

Fig. 9. The relationship between the long diameter and the short diameter at spray angles 75° to 15°.

Table 3. The average and standard deviation of the ratio "a/b" in the experimental results.

Material		Spray Angle φ					
		90°	75°	60°	45°	30°	15°
Nickel	Ratio Average	1.005	1.142	1.180	1.471	2.124	4.506
	Standard Deviation	0.046	0.060	0.044	0.121	0.166	0.482
	Sample Size	52	60	69	59	83	63
Copper	Ratio Average	1.002	1.124	1.157	1.458	2.046	5.459
	Standard Deviation	0.049	0.037	0.039	0.093	0.169	0.335
	Sample Size	10	25	13	21	17	24
Aluminum	Ratio Average	1.001	1.048	1.223	1.495	2.196	4.853
	Standard Deviation	0.038	0.033	0.061	0.084	0.177	0.665
	Sample Size	30	34	38	34	49	38
Alumina	Ratio Average	1.005	1.050	1.189	1.462	2.048	3.984
	Standard Deviation	0.018	0.029	0.048	0.082	0.173	0.759
	Sample Size	87	100	119	85	90	88
Titania	Ratio Average		1.063	1.172	1.435	2.133	4.196
	Standard Deviation		0.029	0.031	0.116	0.108	0.307
	Sample Size		16	15	20	16	19
Zirconia	Ratio Average		1.060	1.198	1.420	1.989	3.734
	Standard Deviation		0.041	0.050	0.148	0.138	0.419
	Sample Size		16	23	24	19	24

mathematical model proposed in our previous study are plotted in the graphs [8]. The model derived an expression that describes the elongation ratio ER as a function of the spray angle φ and a parameter n. The equation is expressed as:

$$ER = \frac{1}{\sqrt{1-\frac{-1+\sqrt{1+576n^4\tan^4\varphi}}{288n^4\tan^4\varphi}}} \qquad (2)$$

The model curve agrees well with the experimental results at spray angles from 90° to 30°; however the theoretical value at 15° is larger than the experimental value, shown Fig. 11 and 12. The drop in splat temperature during flattening may cause this large deviation of the model from the experimental results, because the model assumes that the flattening process is isothermal. The flattening time becomes longer as the spray angle is lowered due to a reduction in the perpendicular velocity with respect to the substrate, that is, splat temperature at a lower angle becomes lower. Lower temperature causes higher viscosity of the molten fluid. The model also assumes that the particle moves relatively faster in the parallel direction to the substrate than in the perpendicular direction. The parameter "n" expresses the degree of resistance for the particle to move in the parallel direction. When the particle viscosity become higher, the ratio of the parallel velocity to the perpendicular velocity may decrease, then the elongation ratio lowers. The change of the viscosity during flattening may affect the elongation ratio. If the viscosity maintains the initial value during splat formation, the ratio could become larger. This may be the reason why the theoretical value becomes larger than the experimental results.

Variation in the experimental results. The standard deviation of the experimental elongation ratio increases as the spray angle decreases; as shown in Table 3 and Fig. 10. This deviation of the experimental elongation ratio increases as the spray angle decreases; as shown in Table 3 and Fig. 10.

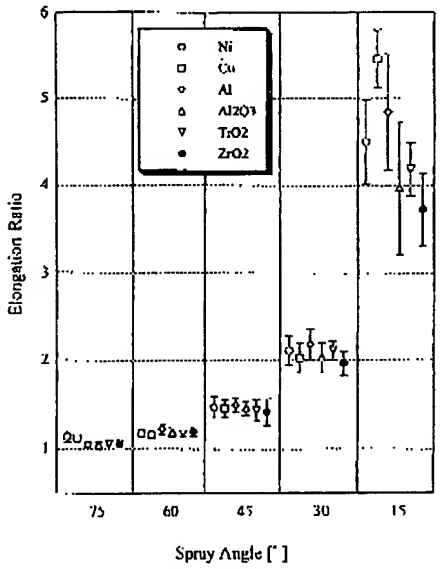

Fig. 10. The average and standard deviation of the elongation ratio at spray angles of 75° to 15° for all materials.

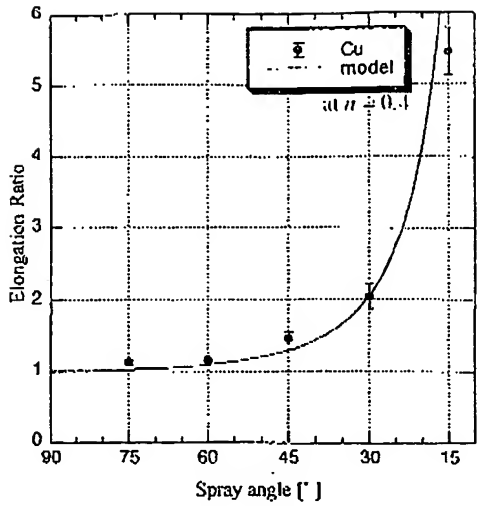

Fig. 11. The relationship between the elongation ratio and the spray angle in Copper spray, and the comparison of the model with experimental results.

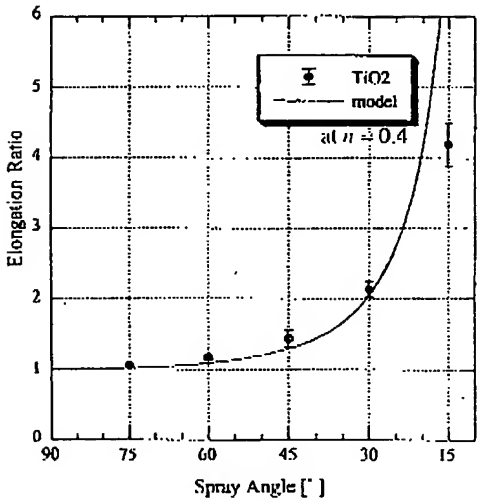

Fig. 11. The relationship between the elongation ratio and the spray angle in Titania spray, and the comparison of the model with experimental results.

This variation originates from broadening of the spray pattern. The particle stream from the plasma nozzle has a broadening angle, as shown in Fig. 13. The particle impact angle changes in the range ϕ to ψ. The difference between the maximum and minimum elongation ratio at spray angle φ is obtained from $ER(\psi)-ER(\phi)$. The next equation holds:

$$ER(\psi)-ER(\phi)=ER(\varphi-\varepsilon)-ER(\varphi+\varepsilon) \qquad (3)$$

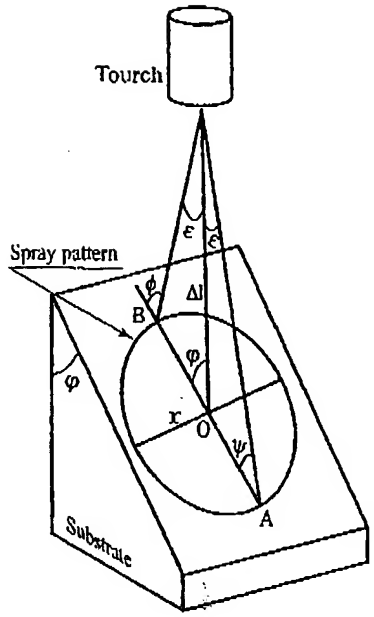

Fig. 13. The broadening powder stream and the variation of impinging angle.

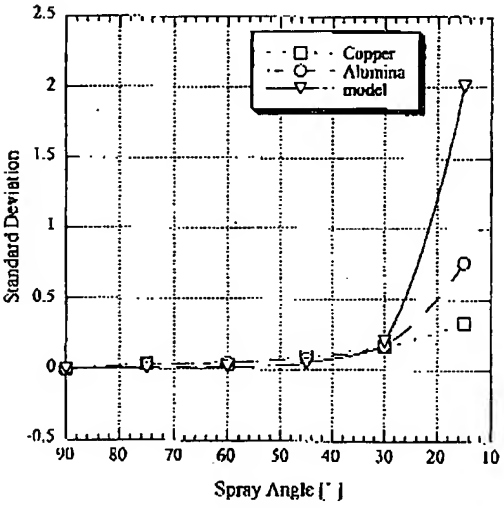

Fig. 14. The comparison of the standard deviation with the variation caused by the broadened particle stream.

because $\phi=\varphi+\varepsilon$ and $\psi=\varphi-\varepsilon$.

The value obtained by substituting $\varepsilon=1°$ into Eq. 3 and the standard deviation in the case of copper and alumina are shown Fig. 14. The variation of the experimental results appears to be explained by the broadened powder stream from the plasma torch.

Conclusions

The splat shape sprayed at off-normal angle is elliptic. In particular, the profiles of the oxide splats were clear and fit an elliptical-shaped footprint quite well. The metal splat contours also agreed with the elliptic curves except for projections peripheral.

The relationship between the major and minor diameters showed strong linearity over the wide range of splat sizes. This implies that the elongation ratio does not depend on the particle diameter and the impact velocity. This behavior appears to validate the model because the model equation does not contain either the particle diameter or the impact velocity explicitly.

The experimental results of the elongation ratio on all the materials were very similar in the range of 90° to 30°. The results at 15° varied and were dependent on the material.

The model agreed well with the elongation ratio of the experimental results in the range between 90° and 30°. The model values were over-estimated than the practical results at spray angles less than 15°.

References

1. M. F. Smith, R. A. Neiser and R. C. Dykhuizen, An Investigation of the Effects of Droplet Impact Angle In Thermal Spray Deposition, Thermal Spray Industrial Applications, Boston, 20-24 June 1994, 603-608.
2. S. H. Leigh and C. C. Berndt, Evaluation of off-angle thermal spray, Surface and Coatings Technology 89 (1997) 213-224.
3. R. C. Tucker, Jr. and M. O. Price, The Effect of Angle of Deposition on The Properties of Selected Detonation Gun Coatings. Proceedings of ATTAC'88, Osaka, Japan, May 1988, 61-71
4. G. Montavon, C. C. Coddet, S.Sampath, H. Herman and C. C. Berndt, Vacuum Plasma Spray Forming of Astroloy, An Investigation of Processing Parameters, Thermal Spray Industrial Applications, Boston, 20-24 June 1994, 469-475.
5. G. Montavon, S.Sampath, C. C. Berndt, H. Herman and C. C. Coddet, Surface and Coatings Technology 91 (1997) 107-115.
6. G. Montavon and C. C. Coddet, 3-D Profilometries of Vacuum Plasma Sprayed Nickel-Based Alloy Splats Using Scanning Mechanical Microscopy, Advances in Thermal Spray Science & Technology, Houston, Texas, 11-15 September 1995, 285-289.
7. V. V. Sobolev and J. M. Guilemany, Droplet Flattening During Thermal Spray at Off-Normal Angles, Thermal Spray (Meeting the Challenges of the 21st Century), Nice, France, 25-29 May 1998, 497-502.
8. H. Fukanuma, C-J. Li, Mathematical modeling of splat formation at off-normal angles in thermal spray, Proceedings of United Thermal Spray Conference, Düsseldorf, Germany, 17-19 March 1999, 513-518.
9. M. Bussmann, S. Chandra, and J. Mostaghimi, Numerical results of off-angle spray particle impact, Proceedings of United Thermal Spray Conference, Düsseldorf, Germany, 17-19 March 1999, 783-786.
10. J. Madejski, Solidification of Droplets on A Cold Surface, Int. J. Heat Mass Transfer Vol. 19 (1976), 1009-1013.
11. H. Fukanuma and A. Ohmori, Behavior of Molten Droplets Impinging on Flat Surface, Proceedings of the Thermal Spray Industrial Applications, Boston, 20-24 June 1994, 563-568.